Structural Understanding of the Allosteric Conformational Change of Cyclic AMP Receptor Protein by Cyclic AMP Binding†

Hyung-Sik Won, T. Yamazaki,‡ Tae-Woo Lee, Mi-Kyung Yoon, Sang-Ho Park, Y. Kyogoku,‡ and Bong-Jin Lee*

College of Pharmacy, Seoul National University, San 56-1, Shinlim-Dong, Kwanak-Gu, Seoul 151-742, Korea

Received January 4, 2000; Revised Manuscript Received August 21, 2000

ABSTRACT: Cyclic AMP receptor protein (CRP) plays a key role in the regulation of more than 150 genes. CRP is allosterically activated by cyclic AMP and binds to specific DNA sites. A structural understanding of this allosteric conformational change, which is essential for its function, is still lacking because the structure of apo-CRP has not been solved. Therefore, we performed various NMR experiments to obtain apo-CRP structural data. The secondary structure of apo-CRP was determined by analyses of the NOE connectivities, the amide proton exchange rates, and the ^{1}H-^{15}N steady-state NOE values. A combination of the CSI-method and TALOS prediction was also used to supplement the determination of the secondary structure of apo-CRP. This secondary structure of apo-CRP was compared with the known structure of cyclic AMP-bound CRP. The results suggest that the allosteric conformational change of CRP caused by cyclic AMP binding involves subunit realignment and domain rearrangement, resulting in the exposure of helix F onto the surface of the protein. Additionally, the results of the one-dimensional [^{13}C]carbonyl NMR experiments show that the conformational change of CRP caused by the binding of cyclic GMP, an analogue of cyclic AMP, is different from that caused by cyclic AMP binding.

Cyclic AMP receptor protein (abbreviated as CRP;[1] also referred to as catabolite gene activator protein, CAP) is well-known as a DNA-binding protein that regulates gene transcription by binding to specific DNA sites, as well as by interacting with RNA polymerase (reviewed in refs *1* and *2*). CRP is a dimeric protein composed of two chemically identical subunits. Each subunit of CRP has a molecular mass of 23 619, as deduced from the nucleotide sequence, and is 209 amino acids long with two cAMP-binding sites (*3*, *4*). In its apo-form, i.e., in the absence of cAMP, CRP is inactive. Upon cAMP binding, CRP is capable of high affinity binding to both DNA and RNA polymerase. The three-dimensional crystal structure of holo-CRP has been solved, in both the presence and absence of DNA (*4*−*9*). However, no structural information about apo-CRP is available. In the crystal structures of holo-CRP, each subunit of CRP is composed of two domains, which are covalently connected by a stretch of polypeptides running between the C helix of the N-terminal domain and the D helix of the C-terminal domain, named the hinge region (Figure 1). The larger N-terminal domain, which is predominantly β-stranded, is for dimerization of CRP and also provides the cAMP binding specificity through a β-roll structure. The smaller C-terminal domain, which is predominantly α-helical, is involved in specific recognition of DNA via a helix-turn-helix motif (E helix and F helix).

Biochemical and biophysical studies have shown that cAMP binding allosterically induces CRP to assume a conformation that binds to DNA and interacts with RNA polymerase (*10*−*19*). In contrast, cGMP, an analogue of cAMP, binds to CRP with an affinity comparable to that of cAMP, but does not induce the binding of the protein to DNA (*11*, *17*−*19*). However, the details of the mechanism by which cAMP mediates the allosteric activation of CRP remain obscure, because the structure of apo-CRP has not been available. To solve this problem, we have studied the solution structure of apo-CRP by NMR spectroscopy. The most important question regarding the mechanism of CRP activation by cAMP is how the signal of cAMP binding is transmitted in the CRP dimer from cAMP-binding domains to DNA-binding domains. At present, two or three models have been proposed, independently or combined with each other, with the concept of "rigid-body movement" (*7*, *20*−*28*). The first model demonstrates that cAMP binding alters the relative orientation of the C, D, and F helices of CRP, positioning the F helix appropriately to interact with DNA. This model was proposed from the characterization of a CRP mutant (*20*, *21*) and is supported by the protein footprinting experiments (*22*, *23*). Similarly, in the second model, the role of cAMP binding to CRP is to alter the relative orientation of the two domains. Consistent with this model,

† This work was partly supported by the Genetic Engineering Research Program (1996), Ministry of Education, Korea.

* To whom correspondence should be addressed. Phone: 82-2-880-7869. Fax: 82-2-872-3632. E-mail: lbj@nmr.snu.ac.kr.

‡ Institute for Protein Research, Osaka University, Japan.

[1] Abbreviations: cAMP, cyclic adenosine mono-phosphate; CD, circular dichroism; cGMP, cyclic guanosine monophosphate; CRP, cyclic AMP receptor protein; CSI, chemical shift index; DNA, deoxyribonucleic acid; DSS, 2,2-dimethyl-2-silapentane-5-sulfonate; ϵ_{278}, extinction coefficient at 278 nm; *E. coli*, *Escherichia coli*; HSQC, heteronuclear single quantum coherence; IPTG, isopropyl-β-D-thiogalactopyranoside; NMR, nuclear magnetic resonance; NOE, nuclear overhauser effect; NOESY, NOE correlated spectroscopy; PMSF, phenylmethanesulfonyl fluoride; RNA, ribonucleic acid; SDS−PAGE, sodium dodecyl sulfate−polyacrylamide gel electrophoresis; TALOS, torsion angle likelihood obtained from shift and sequence similarity; TOCSY, total correlation spectroscopy; TSP, 3-(trimethylsilyl)propionate.

10.1021/bi000012x CCC: $19.00
Published on Web 10/13/2000

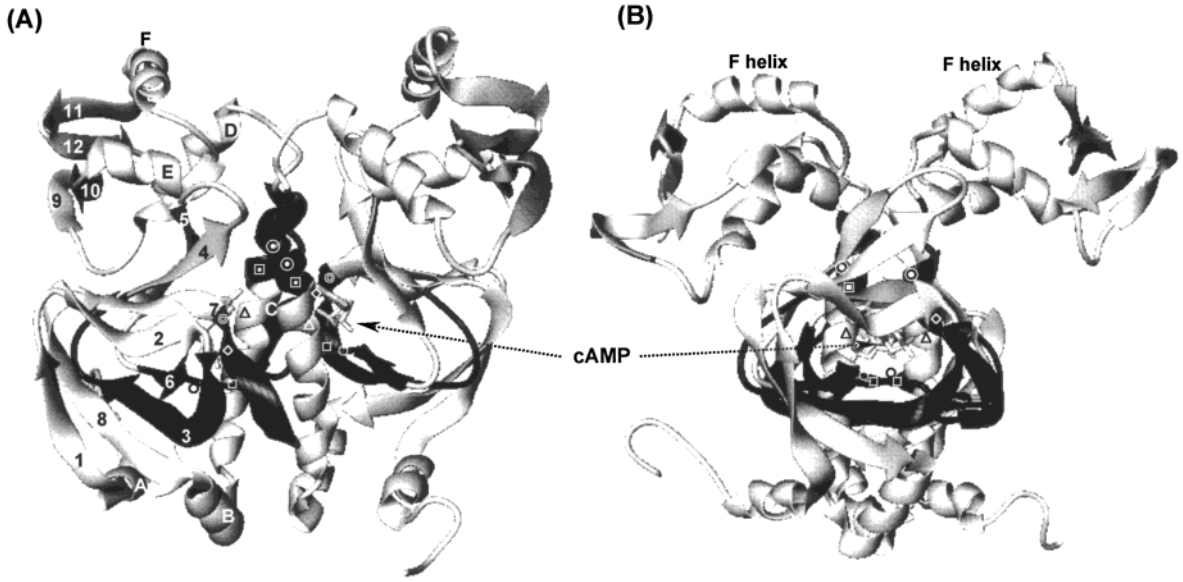

FIGURE 1: Ribbon presentation of the crystal structure of holo-CRP dimer. The direction of view is different between panels A and B, by the relative rotation of the protein by about 90° with the long axis of the C helix. At the center of each subunit, the cAMP molecules bound to the protein are shown as stick-like models. The secondary structure in the subunit is labeled with letters for α-helices and numbers for *β*-strands. The regions showing reasonable differences in secondary structure between apo- and holo-CRP are shadowed in black: E34-V47, D68-S83, and T127-N133. The positions of cAMP-contacting residues are indicated: G71 (○), E72 (□), R82 (◇), S83 (◎), R123 (△), T127 (outlined square), and S128 (⊙). These drawings were produced with the UCSF MidasPlus program using the coordinates for holo-CRP (*7*).

Table 1: [^{13}C-carbonyl,^{15}N-amide]-Double-Labeled Sites for Site-Specific Assignments of the ^{13}C-Carbonyl Carbon Resonances of CRP

target amino acid	double-labeling (−^{13}C−^{15}N−) sites		
[^{13}C]tyrosine	−Tyr23−Pro24−	−Tyr40−Tyr41−	−Tyr41−Ile42−
	−Tyr63−Leu64−	−Tyr99−Lys100−	−Tyr206−Gly207−
[^{13}C]phenylalanine	−Phe14−Leu15−	−Phe69−Ile70−	−Phe76−Glu77−
	−Phe102−Arg103−		−Phe136−Leu137−
[^{13}C]methionine	−Met59−Ile60−	−Met114−Arg115−	−Met120−Ala121−
	−Met157−Thr158−	−Met163−Gln164−	−Met189−Leu190−

several mutational analyses of CRP have suggested a hinge reorientation that adjusts the small domains to interact with DNA (*21*, *24*−*26*). In these two models, the conformational effect induced by cAMP at its binding site is transmitted to the DNA-binding site, mainly in the monomer units, through the hinge region. In contrast, the third model states that the overall realignment of the two subunits within a CRP dimer is crucial for the activation of CRP upon cAMP binding. This model was derived from the investigation of the intersubunit interaction of the CRP dimer mediated by cAMP binding (*21*, *27*−*29*).

Until now, however, no structural data that support the three mechanisms have been reported. This paper presents the secondary structure of apo-CRP in solution, and provides structural evidence for the three mechanisms of CRP activation. We also studied the differences between the binding mode of cAMP to CRP and that of cGMP, by using a [^{13}C]carbonyl NMR technique. Although the three-dimensional structure of apo-CRP is not yet available, our results and investigations provide a detailed structural picture at the atomic level for the allosteric activation of CRP.

EXPERIMENTAL PROCEDURES

Materials. Isotope (^{15}N or ^{13}C)-labeled amino acids, $^{15}NH_4Cl$, and 99.9%-D_2O were purchased from Isotec (Miamisburg, OH) and Cambridge Isotope (Andover, MA). The isotope enrichment was 95% or higher for each of the amino acids. IPTG, cAMP, cGMP, and subtilisin were purchased from Sigma (St. Louis, MO), and all other materials were either analytical or biotechnological grade. Column resins, Bio-Rex 70 and hydroxyapatite were purchased from Bio-Rad Laboratories (Hercules, CA).

Sample Preparation. Uniformly ^{15}N-labeled CRP was prepared from the overproducing *E. coli* strain pp47 containing the plasmid pLCRP1, by growing the bacteria in M9 minimal medium with $^{15}NH_4Cl$ as the sole nitrogen source. Specific amino acid (tyrosine, phenylalanine, or methionine) [^{13}C]carbonyl carbon-labeled CRP and ^{13}C-^{15}N double-labeled proteins were obtained from the overproducing *E. coli* strain BL21 containing the plasmid pT_7−CRP, with the isotope-labeled amino acids. Table 1 shows the kinds of site-specifically double-labeled samples used for the assignments of the carbonyl carbon resonances of the Tyr, Phe, and Met residues. The purification of CRP was performed by sequential chromatography on Bio-Rex 70 and hydroxyapatite, as described previously (*30*). The purity was confirmed by SDS−PAGE, and the concentration of CRP was determined spectrophotometrically with $\epsilon_{278} = 4.1 \times 10^4\ M^{-1}\ cm^{-1}$ for the dimer (*31*). The large-scale preparation of half-size deleted CRP (αCRP) was done according to the method reported previously (*32*). A 19 μg/mL CRP solution in the presence of 1 mM cAMP was digested with 1.2 μg/mL of

subtilisin for 9 min at 37 °C, in a 20 mM potassium phosphate, 370 mM NaCl, pH 7.0 buffer. The reaction was stopped by the addition of PMSF to a 1 mM of final concentration, and the mixture was incubated for an additional 5 min at 37 °C. The mixtures were immediately subjected to cation-exchange chromatography (Bio-Rex 70) for purification. The concentration of the purified αCRP was determined spectrophotometrically with $\epsilon_{278} = 2.6 \times 10^4$ M^{-1} cm^{-1} for the dimer (*31*). The absence of cAMP in the protein solution was checked by the absorbance ratio at 278 and 260 nm (*27*, *33*). Cyclic AMP was easily removed from αCRP after purification through a column chromatography procedure.

NMR Experiments. Uniformly ^{15}N-labeled and nondeuterated apo-CRP was used to record a 3D ^{15}N-edited TOCSY−HSQC spectrum with an isotropic mixing time of 30 ms and a 3D ^{15}N-edited NOESY−HSQC spectrum with a 100 ms mixing time. Slowly exchanging NH protons were monitored with a series of 2D ^{1}H-^{15}N HSQC spectra. The amide-proton exchange experiment was started immediately after the addition of D_2O to a sample of ^{15}N-labeled apo-CRP lyophilized from buffer. The first ^{1}H-^{15}N HSQC experiment was started 10 min after dissolving the sample in D_2O. After the first ^{1}H-^{15}N HSQC experiment, a series of experiments was recorded at 40, 70, 100, 130, 190, 250, 310, 370, 430, and 490 min. The ^{1}H-^{15}N steady-state NOE values were determined from spectra recorded with (NOE experiment) and without (NONOE experiment) a proton presaturation period of three seconds (*34*, *35*). ^{1}H saturation was achieved with the use of 120° ^{1}H pulses applied every 5 ms. In the case of the spectrum without NOE (equilibrium nitrogen magnetization spectrum, NONOE spectrum), a relaxation delay of 5 s was employed, while a relaxation delay of two seconds prior to 3 s of proton presaturation was employed for the NOE spectrum. All of the above-mentioned NMR spectra were obtained at 40 °C on a Bruker DRX 600 spectrometer with the uniformly ^{15}N-labeled and nondeuterated apo-CRP dissolved in 50 mM potassium phosphate buffer (pH 6.0) containing 0.5 M KCl. The spectra were processed and analyzed on a Silicon Graphics Indigo-2 workstation, using the NMRPipe/NMRDraw software (*36*) and the NMRView program (*37*). [^{13}C]Carbonyl NMR spectra were recorded on a Bruker AMX 500 FT NMR spectrometer at 30 °C with the protein dissolved in 50 mM potassium phosphate buffer (pH 6.7) containing 0.3 M KCl. Before measurement, the solvent water was changed to D_2O after lyophilization. Cyclic AMP or cyclic GMP was added as a concentrated stock to a 0.5 mM final concentration. The final concentration was in the range of 0.5−0.7 mM for apo-CRP, and 0.1−0.2 mM for the CRP complexed with cAMP or cGMP. The NMR spectra were recorded at 125 MHz using a Waltz-16 composite pulse decoupling sequence. The free induction decay was recorded with 32 K data points and a spectral width of 25 000 Hz. The ^{13}C chemical shifts are given in parts per million from the methyl group resonance of DSS.

RESULTS

CSI and TALOS. As the number of residues (and thus the number of NOEs) increases, the difficulty in measuring, identifying, and assigning the ^{1}H NOEs grows very rapidly. Furthermore, as the size of the protein increases, the relaxation times progressively shorten and the effects of spin-diffusion make ^{1}H NOE measurements much more difficult to analyze (*38*). Since these problems occurred with CRP (47 kDa), the CSI method and the TALOS program (*39*) were used to determine the secondary structure of apo-CRP. The CSI and TALOS approaches were developed to provide a NOE-independent method for structure determination (*38*, *39*). Since the CSI protocol is fundamentally a statistical technique (*38*) and the TALOS-derived ϕ/φ-values are empirical in nature (*39*), the two applications complement each other. To be applied more correctly to the CSI method and the TALOS program, the chemical shifts of apo-CRP were first adjusted to be referenced to TSP for the ^{13}C atoms and to liquid ammonia for the ^{15}N atoms (*39*). Second, the chemical shifts of the $^{13}C^{\alpha}$, $^{13}C^{\beta}$, and ^{15}N atoms were modified to account for deuterium isotope effects on the atoms (*40*, *41*), since the previous NMR assignments of apo-CRP were done with a highly deuterated sample (*30*); the $^{13}C^{\alpha}$, $^{13}C^{\beta}$, and ^{15}N chemical shifts are moved upfield by the replacement of locally bonded protons with deuterons (*40*, *41*). The CSI results of apo-CRP are shown in Figure 2 along the sequence. The mark "1" represents the β-strand tendency of the atom of the residue (upfield shifts of $^{13}C^{\alpha}$ or $^{13}C'$ resonances, and downfield sfifts of $^{13}C^{\beta}$ resonances from their reference values), while the mark "−1" represents the opposite pattern (α-helical tendency). The chemical shift within the reference value range was marked as a "0". The consensus CSI for each residue was derived by a simple "majority rule" (two or three out of three, ref *38*) from the individual CSI of each ^{13}C atom. In the consensus plot in Figure 2, "1" and "−1" indicate respectively a β-strand and an α-helix tendency of the residue, while the others (zero values) indicate that the residue does not have a strand or a helical tendency. It has been demonstrated that the accuracy of the consensus CSI is in excess of 92%, and many of the errors lie in the N- or C-terminus of helices or strands (*38*). TALOS is a new database system for the prediction of ϕ and φ backbone torsion angles using a combination of chemical shift assignments for a given protein sequence (*39*). The TALOS output for the ϕ and φ angles of the center residue in each string consists of the average of the corresponding angles in the 10 strings in the database with the highest degree of similarity. The individual prediction is classified as "Good" (good prediction with at most one outlier), "Bad" (bad prediction relative to a known structure), "Ambiguous" (no prediction), or "Unclassified" (no classification yet), according to the reliabilities of the prediction. When the chemical shift data of apo-CRP were applied to this program, the predicted backbone angles of 132 residues were classified as "Good", and the others were "Unclassified". No residue was classified as "Bad" or "Ambiguous". In Figure 2, the predicted angles of the residues classified as "Good" are plotted with their standard deviations along the sequence. An advantage of the TALOS approach is that it considers the chemical shifts and the residue types of a string of length 3 instead of only a single residue to obtain the information, and its accuracy was estimated at about 97% (*39*).

NOE Connectivities. The sensitivity and the resolution of the 3D TOCSY−HSQC (30 ms mixing time) and 3D NOESY−HSQC (100 ms mixing time) spectra of the uniformly ^{15}N-labeled and nondeuterated apo-CRP were too

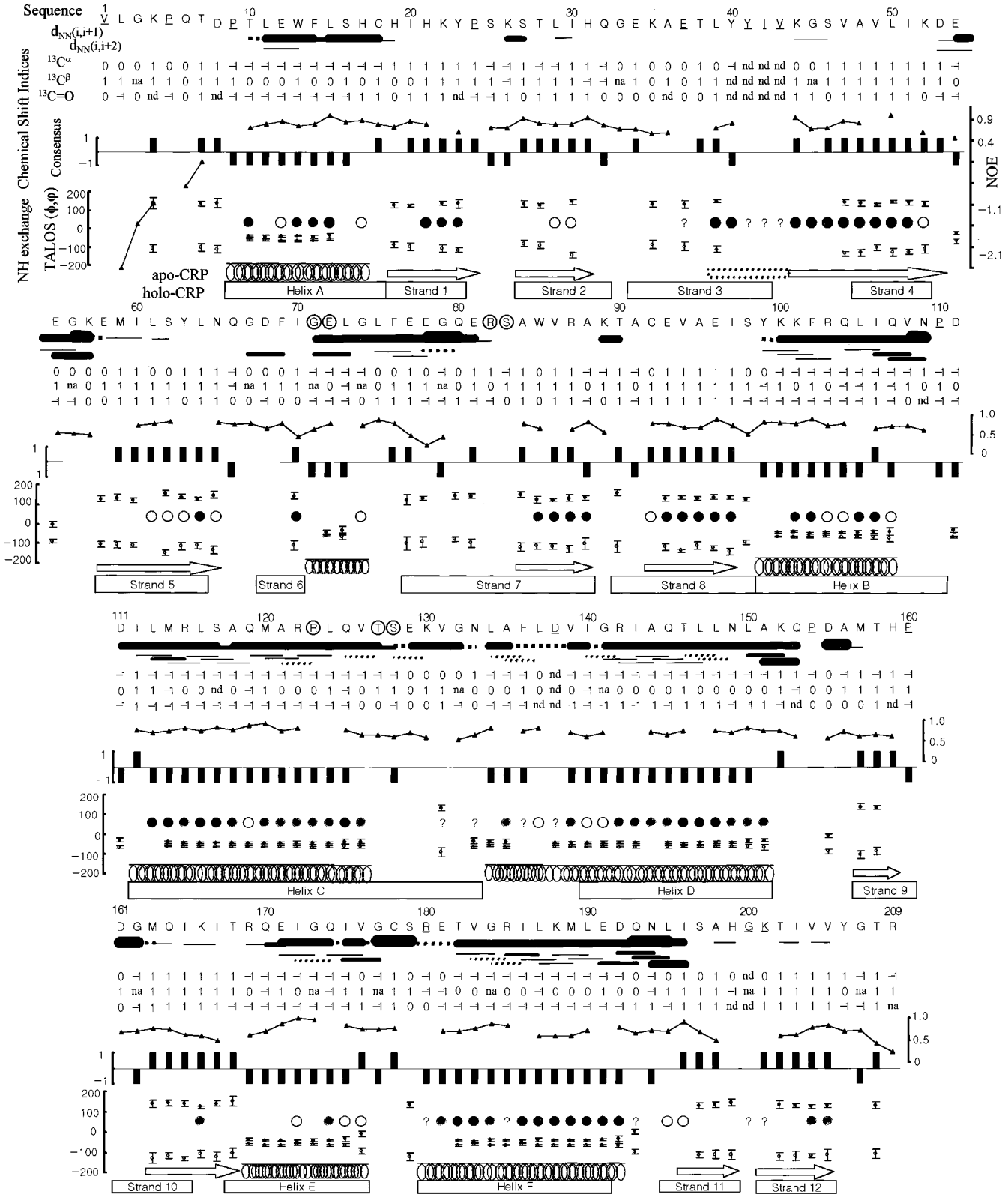

FIGURE 2: Secondary structure determination of apo-CRP. Dashed lines and question marks represent the tentative assignments, due to spectral overlap. For the NOE connectivity data, the height of the bar corresponds to the intensity of the correlation [weak, medium, strong, and very strong for the $d_{NN}(i,i+1)$, weak, medium, or strong for the $d_{NN}(i,i+2)$ cross-peaks]. Refer to the text for the individual and consensus CSI results. "na" and "nd" indicate "not available" and "not detected", respectively. The length of the error bars with the TALOS-predicted backbone angles, ϕ (○) and φ (●), indicates the standard deviation from the average of the dihedral angles of the 10 residues from the database with the highest chemical shift and sequence similarity with the query residues. Triangles correspond to the steady-state ^{1}H-^{15}N NOE values of each residue. Moderately, slowly, and very slowly exchanging amides are represented as open circles, gray circles, and filled circles, respectively. The other residues showed fast exchange of the amide proton. The determined secondary structure elements of apo-CRP are indicated by coil symbols for α-helices and arrow symbols for β-strands. The secondary structure of holo-CRP derived from the analysis by Weber and Steitz (*7*) is represented with boxes. The residues with unavailable $^{1}H^{N}$ and ^{15}N chemical shifts are underlined and those that interact directly with cAMP are marked by open circles in the sequence line.

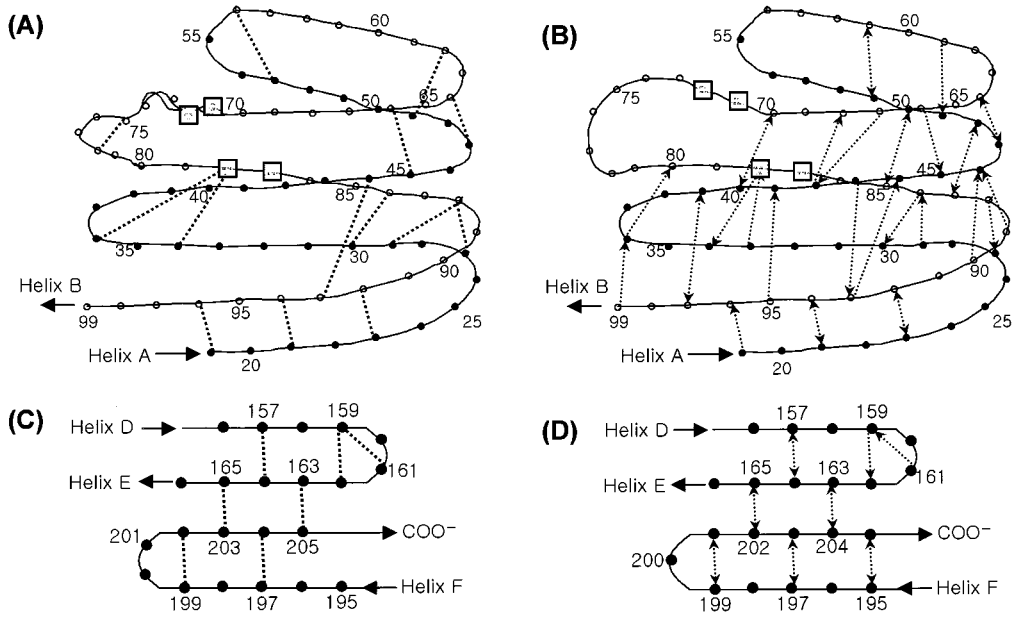

FIGURE 3: Strong long-range NOEs between amide protons (A) in the N-terminal and (C) in the C-terminal β-strands of apo-CRP, and main-chain hydrogen bonds (B) within the N-terminal β-roll structure and (D) within the C-terminal β-sheet of holo-CRP. Every (A and B) fifth or (C and D) second residue is numbered. The direction of the hydrogen bond, H^N to C′, is indicated by an arrow (B and D). The residues that interact directly with cAMP are indicated by boxes (G71, E72, R82, and S83).

low, and the spectral overlap was too serious to be analyzed (data not shown). The reduced resolution and sensitivity of the spectra seem to be due to the high molecular weight of the protein. The molecular weight (47 000) and the rotational correlation time (55 ns, ref *11*) of CRP are so high that low quality spectra seem to be expected without the use of a special technique, such as deuteration. Generally, it has been shown that high quality H^N-H^N NOE spectra can be recorded on a deuterated protein (*42*, *43*). Nearly complete (~90%) deuteration is also needed for the assignments of the backbone NMR signals of a high molecular weight protein (*44*). Thus, we previously used a fully (~90%) deuterated sample to assign the backbone NMR signals of apo-CRP (*30*). Deuteration greatly enhanced the quality of the 3D NOESY−HSQC spectrum of the protein, but the spectrum necessarily lacked the NOE cross-peaks between the protons attached to the carbon atoms. For these reasons, we finely analyzed the NOE connectivities only between the amide protons from the 3D NOESY−HSQC spectrum of the fully (~90%) deuterated apo-CRP, which had been recorded with a 150 ms mixing time (*30*). The sequential and short-range $d_{N,N}(i,i+2)$ connectivities are summarized in Figure 2. The $d_{N,N}(i,i+3)$ connectivities were seldom observed despite the 150 ms mixing time, probably due to the short transverse relaxation time (T_2) expected from the high rotational correlation time (55 ns, ref *11*) of apo-CRP. Mixing times more than 150 ms were not used in this experiment, to avoid spin diffusion (*38*, *45*). About twenty strong NOEs between the amide protons that are distant from each other in the primary structure were detected unambiguously, and are displayed in Figure 3.

Steady State ^{1}H-^{15}N NOE and Backbone Amide Exchange. Since most of the backbone NMR signals of apo-CRP had been assigned by heteronuclear multidimensional NMR spectroscopy (*30*), 195 of the 202 possible backbone amide chemical shifts (209 residues minus six prolines and the N-terminal residue) were available. Nevertheless, only 161 ^{1}H-^{15}N NOE values of the 195 resonances were identified unambiguously, because the peak overlap was extreme in some regions of the 2D NOE and the 2D NONOE spectra (Figure 4). The individual NOE values that were determined are plotted in Figure 2 along the sequence. Negative NOEs appeared only in the N-terminal region, while the C-terminal region did not show negative NOEs, indicating a more constrained structure in this region than in the N-terminal region. The spectral overlap was somewhat alleviated in the amide proton exchange experiment, since about 50% of the signals disappeared immediately in the first ^{1}H-^{15}N HSQC spectrum after solvent exchange from H_2O to D_2O. The slowly exchanging NH groups that were identified are also indicated along the sequence in Figure 2.

Secondary Structure of apo-CRP. In Figure 1, the sequential and short-range NOE connectivities, the NH exchange, the ^{1}H-^{15}N NOE values, and the CSI and TALOS prediction results are summarized. Dashed lines and question marks represent ambiguities due to spectral overlap or unavailable amide chemical shifts. On the basis of all of the results, the secondary structure of apo-CRP was determined as illustrated in Figure 2 (coil symbols for α-helices, and arrow symbols for β-strands). Seven regions were determined as α-helices, where the sequential $d_{NN}(i,i+1)$ NOEs continue strongly, the short-range $d_{NN}(i,i+2)$ NOEs are frequent, the ^{1}H-^{15}N steady state NOE values are relatively high, the amide exchanges are relatively slow, the predicted backbone angles (ϕ and φ) indicate helical properties as judged from the Ramachandran plot (*39*), and the consensus CSIs mainly indicate continuous helical tendencies: P9−H18, G71-G74, and Y99-Q107, I112−V126, (L134)D138-A151, R169−V176, and R180-D192. Although the NOEs between the $^1H^\alpha$ and $^1H^N$ atoms were not available, 10 β-strands were determined, by using different data, where the ^{1}H-^{15}N steady state NOE values and the amide exchanges are relatively high and slow, the sequential $d_{NN}(i,i+1)$ and short-range $d_{NN}(i,i+2)$ NOEs are absent or weak, and the predicted backbone angles and

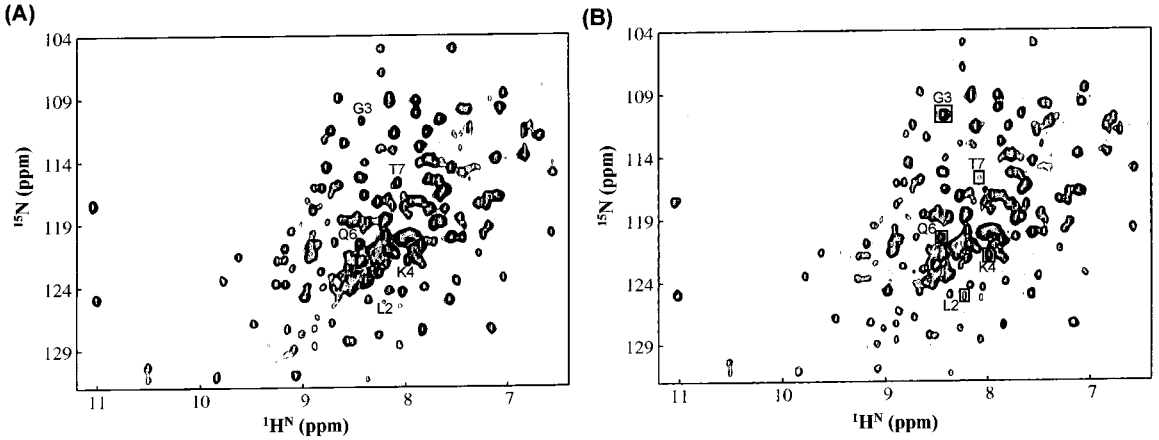

FIGURE 4: 2-D (A) NONOE and (B) NOE spectra of apo-CRP. Negative NOE peaks are labeled with boxes.

consensus CSIs indicate mainly β-strand tendencies: H19−P24, S27−H31, (L39)K44-D53, E58-N65, A84-A88, C92−I97, M157-H159, M163-T168, I196−H199, and K201−V205. The presence of β-strands is also supported by the long-range NOEs between the strands (Figure 3), which allude to the presence of parallel or antiparallel β-sheets. It is not clear, due to a lack of information, whether the residues from Y40 to V43 and from L134 to D138 should be included respectively in the strand and in the helix components (Figure 2).

One-Dimensional ^{13}C-Carbonyl NMR Experiments. To overcome the experimental difficulties in the multidimensional NMR studies on the CRP with ligands, which was noted previously above, we used the one-dimensional [^{13}C]-carbonyl NMR spectroscopy with selective labeling (*46*, *47*) as a simple technique to compare the conformational effects of cGMP on CRP with those of cAMP. To ensure efficient ligand binding (cAMP or cGMP), a lower salt concentration (0.3 M KCl) than that used in the multidimensional NMR experiments for the secondary structure determination of apo-CRP (0.5 M KCl) was applied. Although the concentration of ligand (cAMP or cGMP)-bound protein was rather low (0.1−0.2 mM) to obtain multidimensional NMR spectra, all of the expected resonances could be detected in the one-dimensional spectrum by increasing the experimental time (Figures 5−8). The simplification of the spectra by the selective labeling compensated for the reduced resolution (i.e., increased line broadening) by the ligation of the protein. The assignments of the [^{13}C]carbonyl resonances were obtained using the ^{13}C-^{15}N double-labeling technique with the limited digestion of CRP (*46*). In a [^{13}C-^{15}N]-double-labeled protein, the peak of a [^{13}C]carbonyl carbon is split and/or decreases in intensity due to spin coupling with the amide ^{15}N of the next residue in the sequence (*47*). The limited subtilisin digestion of the CRP dimer in the presence of cAMP produces αCRP, a dimer of the N-terminal domain of CRP, which retains the same structure as found in the intact protein (*14*, *48*). This method made it possible to assign even the carbonyl resonances coupled with proline amides, which could not be assigned by the previous 3D HNCO experiment. Figure 5 shows an example of the assignments of the carbonyl resonances from tyrosine residues. In the [^{13}C]carbonyl NMR spectrum of apo-CRP labeled with ^{13}C-Tyr, the carbonyl resonances of the six tyrosine residues in a subunit of apo-CRP were well resolved, except for the

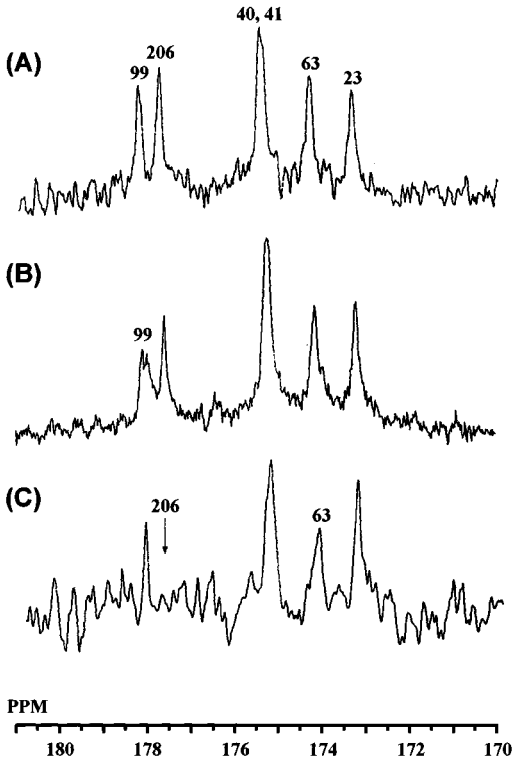

FIGURE 5: 125-MHz [^{13}C]carbonyl NMR spectra of (A) [^{13}C-Tyr]-apo-CRP, (B) [^{13}C-Tyr,^{15}N-Lys]apo-CRP, and (C) [^{13}C-Tyr,^{15}N-Leu]αCRP.

overlap of two peaks in the middle (Figure 5A). The [^{13}C]-carbonyl NMR spectrum of apo-CRP, in which the Tyr and Lys residues were labeled simultaneously with ^{13}C-Tyr and ^{15}N-Lys, showed a doublet signal centered near 179 ppm with the other resonances unsplit (Figure 5B). Since only Tyr 99, of the six tyrosine residues existing in a CRP subunit, is directly followed by lysine, the split peak was unambiguously assigned to Tyr 99 of apo-CRP. When the [^{13}C-Tyr,^{15}N-Leu]CRP was cleaved by subtilisin, a peak disappeared, and therefore it could be assigned to Tyr 206, which is the only residue located in the C-terminal domain of CRP (Figure 5C). In addition, the peak severely decreased in intensity could be assigned to Tyr 63, which is next to Leu 64 (Figure 5C). In this way, we could assign all of the [^{13}C]carbonyl resonances of the Tyr, Phe, and Met residues (Figures 6−8). The chemical shifts of these resonances were in good agreements with those determined previously by the 3D

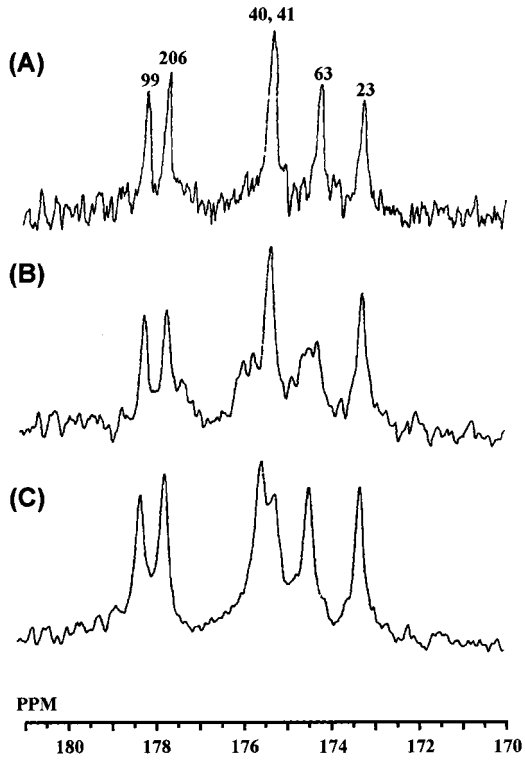

FIGURE 6: 125-MHz [^{13}C]carbonyl NMR spectra of (A) [^{13}C-Tyr]-apo-CRP, (B) [^{13}C-Tyr]CRP in the presence of cAMP, and (C) [^{13}C-Tyr]CRP in the presence of cGMP.

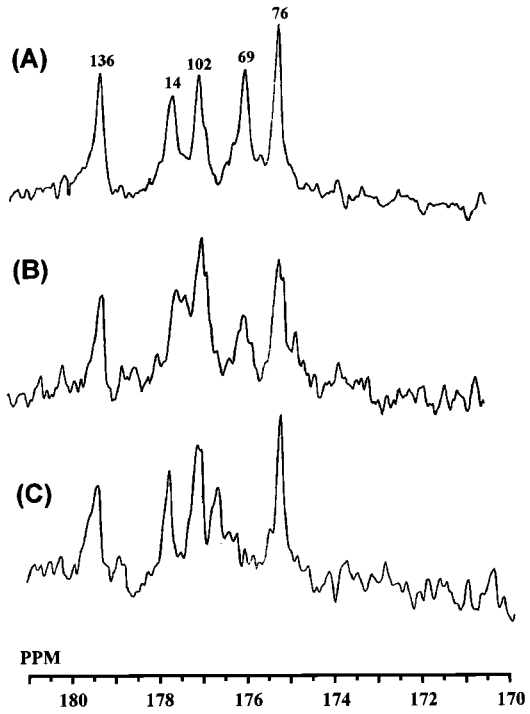

FIGURE 7: 125-MHz [^{13}C]carbonyl NMR spectra of (A) [^{13}C-Phe]-apo-CRP, (B) [^{13}C-Phe]CRP in the presence of cAMP, and (C) [^{13}C-Phe]CRP in the presence of cGMP.

HNCO experiment (*30*). The number of peaks in the [^{13}C]-carbonyl NMR spectra of apo-CRP coincided equally with the number of residues of one subunit (Figures 5−8), indicating a symmetric structure of apo-CRP in solution, consistent with the previous results (*30*). Additionally, the [^{13}C]carbonyl NMR spectra of the αCRP dimer (Figure 5C) showed the unchanged symmetry of the protein in solution,

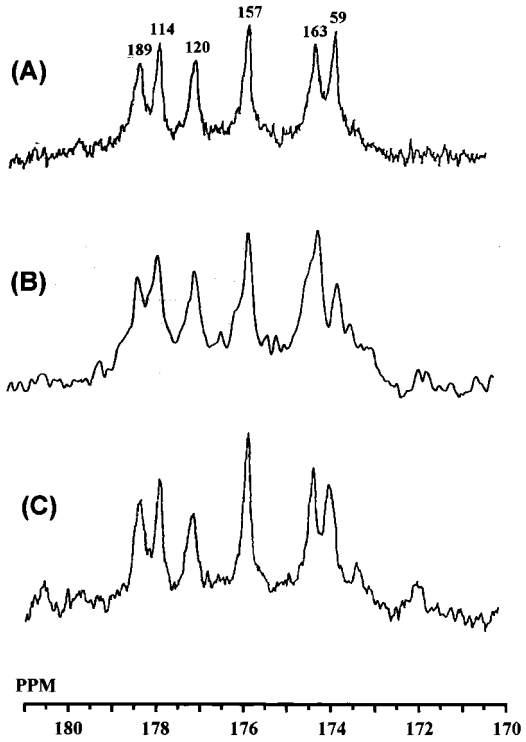

FIGURE 8: 125-MHz [^{13}C]carbonyl NMR spectra of (A) [^{13}C-Met]-apo-CRP, (B) [^{13}C-Met]CRP in the presence of cAMP, and (C) [^{13}C-Met]CRP in the presence of cGMP.

even with the elimination of the small domains. The effects of cAMP on the structure of CRP were studied and compared with those of cGMP binding. When cAMP or cGMP was added to apo-CRP, overall broadening in the [^{13}C]carbonyl NMR spectra occurred, indicating perhaps a motional suppression of the protein by the ligand binding. Despite the overall broadening, some residues of CRP showing certain spectral changes upon cAMP or cGMP binding were identified. The Tyr 63 resonance was remarkably perturbed by the cAMP binding, while either the Tyr 40 or Tyr 41 resonance was shifted slightly upfield upon the addition of cGMP (Figure 6). In the case of the [^{13}C]Phe NMR spectra (Figure 7), the peaks from Phe 69 and Phe 76 were remarkably broadened, and the Phe 136 peak was reduced somewhat as compared to the others by the binding of cAMP. In contrast, the Phe 69 and Phe 136 peaks were broadened slightly and the Phe 69 peak was shifted downfield by the binding of cGMP. As shown in the [^{13}C]Met spectra (Figure 8), the Met 59 peak was changed by the addition of cGMP as well as cAMP. The spectral patterns that changed by cGMP binding were somewhat different from those affected by cAMP binding, meaning that the binding mode and the conformational effects of cGMP to CRP are different from those of cAMP. Additionally, the present [^{13}C]carbonyl NMR experiment reconfirmed that this technique can be used efficiently to study the structural changes of a protein by its interactions with ligands or other proteins.

DISCUSSION

The secondary structure of apo-CRP was determined by the present NMR studies. The allosteric conformational change of CRP upon the binding of cAMP can be understood inevitably by the precise comparison of the structures between apo-CRP and holo-CRP. Accordingly, the present

NMR studies on apo-CRP should be performed similarly with holo-CRP. Unfortunately, however, we failed in this attempt (data not shown), because severe precipitation of CRP occurred when the cAMP was added to 0.6 mM of apo-CRP. After removal of the precipitate, the remaining concentration of CRP was too low to measure the multidimensional NMR signals (severe reduction of the spectral sensitivity), and the spectral line broadening was too extreme to analyze (severe reduction of the spectral resolution). The very low solubility of holo-CRP, which is generally known (*49*), and the motional suppression of CRP by the binding of cAMP (*12*, *15*) may be related to the reduced sensitivity and the spectral line-broadening. Therefore, we compared the NMR-derived secondary structure of apo-CRP in solution with that observed for holo-CRP in the crystal (Figure 2). Of course, it is necessary to refine the determined secondary structure of apo-CRP, particularly in the β-strand components and at the beginning and ending points of each secondary structure element, by a qualitative analysis of the NOEs between the $^1H^\alpha$ and $^1H^N$ atoms; however, this was impossible in the present experiments. Moreover, there is the possibility that some of the observed differences between the two structures are attributable to the different experimental conditions (apo-CRP in solution vs holo-CRP in crystal), particularly in the N- or C-terminus of each secondary structure element. Nevertheless, some regions show reasonable differences between the two secondary structures, from which one can infer the mechanism of CRP activation.

The cAMP-binding domains of holo-CRP provide an example of an ideal β-roll structure (residues H19−Y99, Figures 1 and 3B) that composes the internal cAMP-binding pocket (*7*−*9*). As shown in Figure 2, the region D68−S83, which include four (G71, E72, R82, and S83) of the seven residues (G71, E72, R82, S83, R123, T127, and S128; ref *7*) that interact directly with cAMP, shows relatively large differences between apo-CRP and holo-CRP. On the contrary to holo-CRP, apo-CRP shows no evidence of the presence of β-strands in this region, and instead, the H^N-H^N NOE connectivities suggest the presence of a helix and/or a turn structure in this region of apo-CRP. It is also noteworthy that the residues G71 to G79 are the only part that shows irregularity in the interstrand hydrogen bonding patterns composing the ideal β-roll structure of holo-CRP (Figures 1 and 3B; ref *7*). Accordingly, it seems reasonable that the secondary structure of this region is changed by the direct interaction with the cAMP molecule. The secondary structure of the region E34−V47, which has some ambiguities, also shows a slight difference between apo-CRP and holo-CRP (Figure 2). On the basis of the evidence of hydrogen bonds between residues E34−V47 and residues D68−S83 in holo-CRP (Figures 1 and 3B), the secondary structure of residues E34−V47 also seems to be changed slightly by the cAMP binding, mediated by residues D68−S83. However, the binding of cAMP to CRP does not seem to perturb the global fold of the β-roll structure greatly. Most of the strong long-range H^N-H^N NOEs between the residues in the β-roll of apo-CRP agreed well with the hydrogen bonding patterns between β-strands in that of holo-CRP (Figure 3). The several NOEs (between D53 and G56, between A36 and R82, and between L29 and A88) inconsistent with the hydrogen-bonding patterns could not prove the change in the global fold either, because the distances between the amide nitrogen atoms of the residues, in the crystal structure of holo-CRP, are less than 5 Å, from which strong H^N-H^N NOEs can be expected (*45*). In summary, by the binding of cAMP, the β-roll structure of CRP seems to be slightly perturbed around the cAMP-binding pocket, which seems to be related to only the cAMP-binding property of the protein. None of the present data provide the evidence that the conformational change in this region directly affects the DNA-binding property of CRP. Instead, the signal transmitting the cAMP binding from the cAMP-binding domain to the DNA binding domain seems to be mediated by another region, T127−V139.

In apo-CRP, the residues T127−N133 show few helical tendencies and no slowly exchanging amide protons, while the residues L134−V139 show frequent helical tendencies (Figure 2). However, in holo-CRP, the residues T127−N133 are included in the C helix, while the residues L134−V139 are involved in the interdomain hinge region (Figures 1 and 2). The T127−V139 region contains, at its beginning position, residues T127 and S128, which interact directly with the cAMP molecule (Figure 1; ref *7*). Point mutations at these positions directly affect the activity of CRP (*16*, *28*, *29*, *50*−*52*), indicating that the conformation of this region is crucial for the allosteric activation of CRP. The direct interaction between cAMP and residues T127 and S128 seems to change the secondary structure of the region T127−V139. As many of the intersubunit and interdomain communications of CRP occur in the region T127−V139 (*7*−*9*, *27*), the apparently small conformational change in this region can necessarily alter the relative orientations of the subunits and the domains of CRP. This supports the subunit realignment and domain reorientation as the mechanisms of CRP activation (*20*−*28*). The most important result of these rigid-body movements has been suggested to be the exposure of the F helix, which contacts the DNA directly in the presence of cAMP, onto the surface of the protein (*7*−*9*, *20*−*28*). The present NMR results also support the exposure of the F helix as a result of CRP activation. Although the location and the length of the F helix of apo-CRP were determined to be nearly identical to those of holo-CRP (Figure 2), most of the amide protons in the F helix of apo-CRP were not exchanged after about 6 h, despite the high temperature, 40 °C. The relative convergence of residues with very slow amide exchange rate on the F helix, which is located on the surface of holo-CRP (Figure 1), indicates that the element is probably buried in the core of apo-CRP. For the same reason, the region L39−I51 of apo-CRP also seems to be located in the core of apo-CRP, which is consistent with the case of holo-CRP (Figure 1; refs *7*−*9*).

Figures 3C and 3D show an additional small difference between the apo-CRP and holo-CRP structures. Since it is well ordered, the strong H^N-H^N NOE pattern in Figure 3C seems to reflect directly the hydrogen bonding pattern forming an antiparallel β-sheet of four β-strands in apo-CRP. If this is true, then the hydrogen bonding pattern forming the β-sheet would be very similar, but slightly different, between apo-CRP and holo-CRP; i.e., the residues K201−V205 of apo-CRP would be shifted by one residue relative to those of holo-CRP in their hydrogen-bonding pairs. Additionally, as shown in Figure 2, the position and the length of the β-strand from M163 to T168 of apo-CRP differ

somewhat from those of the corresponding β-strand 10 of holo-CRP. Although several residues in this β-sheet contribute to the direct interaction between CRP and DNA (*8*−*9*, *53*), it is not clear whether these small differences are related to the conformational change of CRP induced by cAMP binding. As many of the residues in this β-sheet show higher temperature B-factors than average in the crystal structure of holo-CRP (*7*), their conformational differences between apo-CRP and holo-CRP may be due to the different conditions of the two (solution vs crystal). Indeed, differences between crystal and solution structures are often reported in regions with high-temperature B-factors in X-ray structures (*39*, *43*).

Cyclic GMP, an analogue of cAMP, cannot activate CRP, although its binding affinity is comparable to that of cAMP (*11*, *17*−*19*). From the present [^{13}C]carbonyl NMR experiments (Figures 6−8), it was confirmed that the effect of cGMP on the structure of CRP is different from that of cAMP. As noted above, the direct interaction between cAMP and the residues T127 and S128 is crucial for the allosteric activation of CRP. This interaction essentially requires the 6-amino group of the adenine ring of cAMP (*7*, *19*). Since the 6-keto group in the guanine ring of cGMP replaces the 6-amino group of cAMP, cGMP binding could not activate CRP.

CONCLUSIONS

The secondary structure of apo-CRP was determined by various multidimensional heteronuclear NMR experiments. From the comparison of the secondary structure between apo-CRP and holo-CRP, the following mechanisms of CRP activation by the cAMP binding were revealed. The structure around the cAMP-binding pocket of CRP is perturbed by cAMP binding, which contributes to the binding affinity of cAMP. The two subunits are realigned and the domains of CRP are reoriented by the conformational change around the hinge region. As a consequence of this global conformational change, the F helices previously buried in the core of the protein become exposed on the surface to bind appropriately to DNA. Additionally, the one-dimensional [^{13}C]carbonyl NMR spectroscopy confirmed that the effect of cGMP binding on the structure of CRP is different from that of cAMP binding.

ACKNOWLEDGMENT

We would like to thank Prof. Hiroji Aiba, of Nagoya University, for his generous gift of the CRP gene. We also thank Miss N. Oda and Mr. K. Teruya for assistance in setting up the growth conditions for *E. coli* in D_2O. We are also grateful to F. Delaglio and Dan Garrett for supplying the NMRPipe/NMRDraw software and the TALOS program, and Bruce A. Johnson (Merck Inc.) for supplying the NMRView program. Finally, we thank the Computer Graphics laboratory (University of California, San Francisco) for supplying the MidasPlus program.

REFERENCES

1. Botsford, J. L., and Harman, J. G. (1992) *Microbiol. Rev. 56*, 100−122.
2. Kolb, A., Busby, S., Buc, H., Garges, S., and Adhya, S. (1993) *Annu. Rev. Biochem. 62*, 749−795.
3. Aiba, H., Fujimoto, S., and Ozaki, N. (1982) *Nucleic Acids Res. 10*, 1345−1361.
4. Passner, J. M., and Steitz, T. A. (1997) *Proc. Natl. Acad. Sci. U.S.A. 94*, 2843−2847.
5. McKay, D. B., and Steitz, T. A. (1981) *Nature 290*, 744−749.
6. McKy, D. B., Weber, I. T., and Steitz, T. A. (1982) *J. Biol. Chem. 257*, 9518−9524.
7. Weber, I. T., and Steitz, T. A. (1987*) J. Mol. Biol. 198*, 311−326.
8. Schultz, S. C., Shields, G. C., and Steitz, T. A. (1991) *Science 253*, 1001−1007.
9. Parkinson, G., Wilson, C., and Gunasekera, A., Ebright, Y. W., Ebright, R. E., and Berman, H. M. (1996) *J. Mol. Biol. 260*, 395−408.
10. Krakow, J. S., and Pastan, I. (1973) *Proc. Natl. Acad. Sci. U.S.A. 70*, 2529−2533.
11. Wu, F. Y.-H., Nath, K., and Wu, C.-W. (1974) *Biochemistry 13*, 2567−2572.
12. Kumar, S. A., Murthy, N. S., and Krakow, J. S. (1980) *FEBS Lett. 109*, 121−124.
13. Lee, B. J., Lee, S. J., Hayashi, F., Aiba, H., and Kyogoku, Y. (1990) *J. Biochem. 107*, 304−309.
14. Sixl, F., King, R. W., Bracken, M., and Feeney, J. (1990) *Biochem. J. 266*, 545−552.
15. Heyduk, E., Heyduk, T., and Lee, J. C. (1992) *J. Biol. Chem. 267*, 3200−3204.
16. Leu, S. F., Baker, C. H., Lee, E. J., and Harman, J. G. (1999) *Biochemistry 38*, 6222−6230.
17. Wu, C.-W., and Wu, F. Y.-H. (1974) *Biochemistry 13*, 2573−2578.
18. Takahashi, M., Blazy, B., and Baudras, A. (1980) *Biochemistry 19*, 5124−5130.
19. Ebright, R. H., LeGrice, S. F. J., Miller, J. P., and Krakow, J. S. (1985) *J. Mol. Biol. 182*, 91−107.
20. Garges, S., and Adhya, S. (1985) *Cell 41*, 745−751.
21. Garges, S., and Adhya, S. (1988) *J. Bacteriol. 170*, 1417−1422.
22. Baichoo, N., and Heyduk, T. (1997) *Biochemistry 36*, 10830−10836.
23. Baichoo, N., and Heyduk, T. (1999) *Protein Sci. 8*, 518−528.
24. Cheng, X., and Lee, J. C. (1998) *Biochemistry 37*, 51−60.
25. Kim, J., Adhya, S., and Garges, S. (1992) *Proc. Natl. Acad. Sci. U.S.A. 89*, 9700−9704.
26. Ryu, S., Kim, J., Adhya, S., and Garges, S. (1993) *Proc. Natl. Acad. Sci. U.S.A. 90*, 75−79.
27. Heyduk, E., Heyduk, T., and Lee, J. C. (1992) *Biochemistry 31*, 3682−3688.
28. Cheng, X., Kovac, L., and Lee, J. C. (1995) *Biochemistry 34*, 10816−10826.
29. Cheng, X., and Lee, J. C. (1998) *J. Biol. Chem. 273*, 705−712.
30. Won, H.-S., Yamazaki, T., Lee, T.-W., Jee, J.-G., Yoon, M.-K., Park, S.-H., Otomo, T., Aiba, H., Kyogoku, Y., and Lee, B.-J. (2000) *J. Biomol. NMR. 16*, 79−80.
31. Takahashi, M., Gronenborn, A. M., Clore, G. M., Blazy, B., and Baudras, A. (1982) *FEBS Lett. 139*, 37−40.
32. Blazy, B., and Ullmann, A. (1986) *J. Biol. Chem. 261*, 11645−11649.
33. Tsugita, A., Blazy, B., Takahashi, M., and Baudras, A. (1982) *FEBS Lett. 144*, 304−308.
34. Farrow, N. A., Muhandiram, R., Singer, A. U., Pascal, S. M., Kay, C. M., Gish, G., Shoelson, S. E., Pawson, T., Forman-Kay, J. D., and Kay, L. E. (1994) *Biochemistry 33*, 5984−6003.
35. Jeon, Y. H., Yamazaki, T., Otomo, T., Ishihama, A., and Kyogoku, Y. (1997) *J. Mol. Biol. 267*, 953−962.
36. Delaglio, F., Grzesiek, S., Vuister, G. W., Zhu, G., Pfeifer, J., and Bax, A. (1995) *J. Biomol. NMR. 6*, 277−293.
37. Johnson, B. A., and Blevins, R. A. (1994) *J. Biomol. NMR. 4*, 603−614.
38. Wishart, D. S., and Sykes, B. D. (1994) *J. Biomol. NMR 4*, 171−180.

39. Cornilescu, G., Delaglio, F., and Bax, A. (1999) *J. Biomol. NMR. 13*, 289−302.
40. Gardner, K. H., Rosen, M. K., and Kay, L. E. (1997) *Biochemistry 36*, 1389−1401.
41. Shan, X., Gardner, K. H., Muhandiram, D. R., Kay, L. E., and Arrowsmith, C. H. (1998) *J. Biomol. NMR. 11*, 307−318.
42. Torchia, D. A., Sparks, S. W., and Bax, A. (1988) *J. Am. Chem. Soc. 110*, 2320−2321.
43. McCallum, S. A., Hitchens, T. K., and Rule, G. S. (1999) *J. Mol. Biol. 285*, 2119−2132.
44. Shan, X., Gardner, K. H., Muhandiram, D. R., Rao, N. S., Arrowsmith, C. H., and Kay, L. E. (1996) *J. Am. Chem. Soc. 118*, 6570−6579.
45. Fogh, R. H., Schipper, D., Boeleus, R., and Kaptein, R. (1995) *J. Biomol. NMR. 5*, 259−270.
46. Han, H.-Y., Lee, Y.-H., Oh, J.-Y., Na, D.-S., and Lee, B.-J. (1998) *FEBS Lett. 425*, 523−527.
47. Kainosho, M., and Tsuji, T. (1982) *Biochemistry 21*, 6273−6279.
48. Clore, G. M., and Gronenborn, A. M. (1982) *Biochemistry 21*, 4048−4053.
49. Ghosaini, L. R., Brown, A. M., and Sturtevant, J. M. (1988) *Biochemistry 27*, 5257−5261.
50. Lee, E. J., Glasgow, J., Leu, S.-F., Belduz, A. O., and Harman, J. G. (1994) *Nucleic Acids Res. 22*, 2894−2901.
51. Gorshkova, I., Moore, J. L., McKenney, K. H., and Schwarz, F. P. (1995) *J. Biol. Chem. 270*, 21679−21683.
52. Shi, Y., Wang, S., Krueger, S., and Schwarz, F. P. (1999) *J. Biol. Chem. 274*, 6946−6956.
53. Lee, B. J., Aiba, H., and Kyogoku, Y. (1991) *Biochemistry 30*, 9047−9054.

BI000012X